Chemical Engineering Science 122 (2015) 403–415

Contents lists available at ScienceDirect

Chemical Engineering Science

journal homepage: www.elsevier.com/locate/ces

Numerical investigation and modeling of reacting gas-solid flows in the presence of clusters

Jesse Capecelatro *, Perrine Pepiot, Olivier Desjardins

Sibley School of Mechanical and Aerospace Engineering, Cornell University, Ithaca, NY 14853, USA

HIGHLIGHTS

- Clusters delay the conversion process by up to 85% compared to a homogeneous flow.
- The PDF of particle-phase volume fraction resembles a lognormal distribution.
- A 0D model that solves the temporal evolution of reactant mass fraction is derived.
- A presumed-shape PDF models the effects of clusters on reactant mass fraction.

ARTICLE INFO

Article history:
Received 26 July 2014
Received in revised form
24 September 2014
Accepted 2 October 2014
Available online 13 October 2014

Keywords:
Gas-solid
Heterogeneous reaction
Fluidized bed
Cluster
Eulerian–Lagrangian
PDF modeling

ABSTRACT

This work presents a volume-filtered formulation for describing chemically reacting flows in the presence of solid catalytic particles. The equations are discretized in a Eulerian–Lagrangian framework and applied to flows of isothermal, heterogeneously reacting chemical species in fully developed three-dimensional risers. The aim of this study is to identify and quantify the influence of particle clusters on heterogenous reactions. The Archimedes number, Ar, is varied from 500 to 12,500, and the Damköhler number, Da, from 0.1 to 10. To assess the multiphase dynamic effects on the chemistry, conversion times from the three-dimensional simulations are compared to a zero-dimensional model that solves for the temporal evolution of the species mass fraction and ignores all spatial variations. The conversion process associated with the three-dimensional simulations is shown to be significantly longer compared to the zero-dimensional solution, with an increasing effect for larger values of Da. The discrepancies can be fully attributed to the presence of clusters, which are accounted for in the zero-order equations by an additional term that contains the covariance between species mass fraction and particle volume fraction fluctuations, which needs to be modeled. To this purpose, contributions to the fluctuating chemical source term are evaluated from the three-dimensional data and discussed, and a presumed-shape probability distribution function (PDF) approach is investigated. This PDF approach models the fluctuating chemical source term by a product of a beta distribution for the species mass fraction and a lognormal distribution for the particle concentration, and yields a mean species solution that agrees very well with the three-dimensional results for the range of Ar and Da considered in this study.

1. Introduction

Reactive gas-solid flows play a major role in a wide variety of engineering devices. Within the energy sector, such flows are used in fluidized bed reactors due to their low pressure drops, uniform temperature distribution, and high efficiency in mixing. Since the 1970s, circulating fluidized bed (CFB) reactors have been used in a range of technical processes, including fluid catalytic cracking (FCC) (Avidan et al., 1990; Avidan, 1996), gasification and combustion of coal (Brereton, 1996; Lee, 1996; Basu, 2006), and more recently thermochemical conversion of biomass (Li et al., 2004; Sanz and Corella, 2006). Currently, catalytic-like processes (e.g., FCC) remain the primary conversion technique within the petrochemical industry (Speight, 2014), and is the focus of this study. A common feature of all reactive gas-solid systems is the complex processes occurring at the particle scale, referred heretofore as microscale processes. These include heat and mass transfer between the two phases, adsorption on and desorption from the solid surfaces, and the actual chemical reaction between the adsorbed gas and the solid (Szekely et al., 1976). If the variations in particle concentration becomes

* Corresponding author.
E-mail address: jsc359@cornell.edu (J. Capecelatro).

http://dx.doi.org/10.1016/j.ces.2014.10.005
0009-2509/

significant, the multiphase dynamics might impact the microscale processes significantly and therefore cannot be ignored. Within the riser of a CFB reactor, solid particles are pneumatically conveyed by a carrier gas phase, characterized by velocities much higher than minimum fluidization. The high flow rates encountered in risers often lead to the spontaneous generation of densely packed particles, referred to as clusters. Clusters have been observed to reduce mixing and interaction of particles with the transport gas (Shaffer et al., 2013), and therefore may inhibit the chemical conversion process, potentially lowering operating efficiencies significantly. Simultaneously accounting for both the microscale processes and particle dynamics poses significant challenges in developing predictive models. As a result, detailed studies demonstrating the quantitative impact of particle clustering on chemical processes occurring in such flows are severely limited.

Due to the importance of reactive gas-solid flows in industrial units and the large impact clusters have on operation efficiency, there exists great need for improved models that account for the presence of clusters during the design process. To this end, we wish to perform high fidelity simulations with the ultimate goal of extracting information that can be used to develop a predictive reduced-order model. In general, simulating chemical processes in fluidized bed reactors requires a chemical kinetic model to describe the various reactions taking place and a framework for solving gas-solid flows. In the context of catalytic cracking in risers, most work found in the literature models the solid phase as a continuous Eulerian field, greatly reducing the computational cost as individual particles do not need to be tracked (see e.g., Theologos and Markatos, 1993; Derouin et al., 1997; Treece et al., 1999; Gupta and Subba Rao, 2001; Das et al., ; Souza et al., 2006; Wu et al., 2008; Prasad Vegendla et al., 2012). In the limit where the flow is highly collisional and assumed to be nearly at equilibrium, the particle density function is close to Maxwellian and a Chapman–Enskog expansion can be used to derive a two-fluid model (TFM) using ensemble or volume averaging (Gidaspow, 1994; Zhang and Prosperetti, 1994; Peirano and Leckner, 1998). However, due to the strong coupling between the gas phase and solid particles, the solid concentration becomes highly segregated and the velocity distribution deviates far from equilibrium. Agrawal et al. (2001) demonstrated that global statistics obtained from Eulerian–Eulerian simulations of non-reactive riser reactors were strongly dependent on the mesh size but became mesh-independent when mesh size is of the order of a few particle diameters. As a result, accurate predictions obtained from TFM are potentially still excessively expensive for such flows. In a recent study, Ozel et al. (2013) employed TFM at various resolutions to obtain mesh-independent results in non-reactive CFB reactors. It was shown that various sub-grid terms have to be modeled in order to account for the unresolved clustering dynamics.

Eulerian–Lagrangian strategies provide an alternative framework that typically relies on simpler closures, where individual particle trajectories are solved using Newton's laws of motion, and models are required for interphase exchange and particle collisions. Because of the added computational expense of tracking individual particles, Eulerian–Lagrangian methods coupled with a chemistry model have only recently been applied in three dimensions (Bruchmüller et al., 2012; Li et al., 2013), but are typically limited to two-dimensional flows with a relatively small number of particles (e.g., Fletcher et al., 2000; Papadikis et al., 2009; Oevermann et al., 2009; Rabinovich et al., 2010; Wu et al., 2010). It has been demonstrated in recent work that two-dimensional simulations are only capable of capturing qualitative features of particle clustering in non-reactive flows, while a fully three-dimensional description is required to accurately capture the quantitative flow behavior (Capecelatro et al., 2014a; Li et al., 2014). In particular, it was shown in our previous work that three-dimensional Eulerian–Lagrangian simulations are capable of accurately reproducing key cluster characteristics, including fall velocity, mean cluster concentration, and concentration fluctuations in risers (Capecelatro et al., 2014a).

The objective of this study is to characterize and quantify the influence of particle clusters on heterogenous reactions in systems that are applicable to a wide range of industrial systems. Fully developed three-dimensional risers are simulated via a Eulerian–Lagrangian approach, where heterogeneous reactions between the solid particles and the carrier gas phase take the form of source terms that are functions of the local solid concentration. The particles are represented as rigid spheres of diameter d_p that are significantly denser than the surrounding fluid, and heat transfer at the particle surface is neglected. In Section 2, we present a volume-filtered formalism for describing heterogenous reactions between individually tracked solid particles and the carrier gas phase. Statistics from the fully developed, three-dimensional risers are presented in Section 3. In Section 4, results from the three-dimensional simulations are compared to a zero-dimensional model that solves for the temporal evolution of the average chemical species mass fraction and neglects all spatial variations. Due to non-linearities in the scalar transport equation, the zeroth-order model contains a term involving the covariance between species mass fraction and particle volume fraction fluctuations. This term accounts for the effects on the chemical processes of the inhomogeneities (i.e., clusters) present in the flow and needs to be modeled. A transport equation for the fluctuating chemical source term is derived and the various contributions are presented and discussed. Finally, a presumed-shape PDF model is proposed for closure of the fluctuating chemical source term and its validity is evaluated.

2. Volume filtered formalism for chemically reacting flows

2.1. Transport of reactive scalars

The transport of mass fraction $0<\hat{Y}\leq 1$ of a chemical reactant can be fully described by

$$\frac{\partial \hat{\rho}_f \hat{Y}}{\partial t}+\nabla\cdot\left(\hat{\rho}_f \hat{Y}\hat{\boldsymbol{u}}_f\right)=\nabla\cdot\left(\hat{\rho}_f\hat{\mathcal{D}}\nabla\hat{Y}\right), \tag{1}$$

where the notation $\hat{(\cdot)}$ denotes a pointwise (i.e., microscale) property of the fluid phase, t is time, $\hat{\rho}_f$ is the fluid density, $\hat{\boldsymbol{u}}_f$ is the fluid velocity, and $\hat{\mathcal{D}}$ is the diffusion coefficient. Note that because only heterogeneous reactions are considered, Eq. (1) does not contain a source term for gas-phase reactions. Instead, adsorption and desorption that occur during the chemical reaction are represented as flux boundary conditions at the particle surface. In order to formulate a tractable system of equations that does not require resolving the flow at the particle scale, a separation of length scales must be established. To achieve this, a volume filtering kernel G is introduced, such that the local mean value A of any microscale quantity $\hat{A}$ is given by

$$\varepsilon_f A(\boldsymbol{x},t)=\int_{V_f}\hat{A}(\boldsymbol{y},t)G(|\boldsymbol{x}-\boldsymbol{y}|)\,d\boldsymbol{y}, \tag{2}$$

where ε_f is the fluid-phase volume fraction, $\boldsymbol{y}$ is the location of the pointwise quantity $\hat{A}$, and $\boldsymbol{x}$ is the local coordinate system of the volume-filtered variables. Applying the volume filter to Eq. (1) yields

$$\frac{\partial}{\partial t}\left(\varepsilon_f\rho_f Y\right)+\nabla\cdot\left(\varepsilon_f\rho_f\boldsymbol{u}_f Y\right)=\varepsilon_f\nabla\cdot\left(\rho_f\mathcal{D}\nabla Y\right)-\nabla\cdot\boldsymbol{R}_Y+\dot{\omega}, \tag{3}$$

where ρ_f, Y, $\boldsymbol{u}_f$, and $\mathcal{D}$ are the volume filtered fluid-phase quantities. A full description of the mathematical derivation can be found in our previous work (Capecelatro and Desjardins, 2013).

In Eq. (3), $\boldsymbol{R}_Y$ is the subfilter scalar flux, similar to the subgrid scalar flux that appears for example in large-eddy simulations (LES) of turbulent combustion, but in this case the unresolved fluctuations may arise from interactions with particles due for example to wakes and interparticle collisions, as opposed to unresolved turbulence fluctuations generated by large-scale energy-containing eddies. Proper closure for this term requires further investigation and is beyond the scope of this work. However, because the chemical reactants do not feed back to the gas-solid flow, and because the majority of fluid velocity fluctuations are assumed to be generated by clusters of particles that are sufficiently resolved by the computational mesh, $\boldsymbol{R}_Y$ is neglected in this study.

Volume filtering the last term in Eq. (1) and assuming that diffusion occurs uniformly over the surface of each particle yields additional subfilter surface contributions. Such contributions include a subfilter diffusion flux that accounts for enhanced or reduced scalar mixing due to the presence of particles. Modeling multicomponent diffusion aspects in fluidized beds is challenging and often neglected in practical studies (Derksen, 2014). Recent work conducting particle-resolved DNS have observed that scalar spreading increases with decreasing solids volume fraction, and increases with increasing particle Reynolds number (Derksen, 2008, 2014), though detailed models that capture these effects are non-existent. However, with sufficient resolution, Eulerian–Lagrangian methods should be adequate in capturing the majority of the diffusion process. The subfiltered surface contributions also account for the heterogeneous reactions that need to be modeled. In order to mimic a catalytic-like process, the chemical reaction between the solid particles and carrier gas phase take the form of a source term in Eq. (3), and the depletion of species mass fraction occurs at a rate $\dot{\omega}$ given by

$$\dot{\omega} = -\varepsilon_f \rho_f Y k \varepsilon_p / \varepsilon_{p,0}, \tag{4}$$

where $\varepsilon_{p,0} = 0.634$ is the random close-packing limit for monodisperse spherical particles (Scott and Kilgour, 1969), and k is a coefficient that controls the rate of reaction.

2.2. Gas phase description

The volume-filtered continuity equation for a variable density, low Mach number flow is given by

$$\frac{\partial}{\partial t}\left(\varepsilon_f \rho_f\right) + \nabla \cdot (\varepsilon_f \rho_f \boldsymbol{u}_f) = 0, \tag{5}$$

and the gas-phase momentum equation is given by

$$\frac{\partial}{\partial t}\left(\varepsilon_f \rho_f \boldsymbol{u}_f\right) + \nabla \cdot \left(\varepsilon_f \rho_f \boldsymbol{u}_f \boldsymbol{u}_f\right) = \nabla \cdot (\boldsymbol{\tau} - \boldsymbol{R}_u) + \varepsilon_f \rho_f \boldsymbol{g} - \boldsymbol{F}^{\text{inter}} + \boldsymbol{F}^{\text{mfr}}, \tag{6}$$

where $\boldsymbol{g}$ is the gravity vector, $\boldsymbol{F}^{\text{inter}}$ is the interphase exchange term, which will be described in detail in Section 2.4, and $\boldsymbol{F}^{\text{mfr}}$ is a source term to maintain a constant mass flow rate for statistically stationary flows. In Eq. (6), the filtered stress tensor, $\boldsymbol{\tau}$, is expressed as

$$\boldsymbol{\tau} = -p\boldsymbol{I} + \mu\left[\nabla \boldsymbol{u}_f + \nabla \boldsymbol{u}_f^{\mathsf{T}} - \frac{2}{3}\left(\nabla \cdot \boldsymbol{u}_f\right)\boldsymbol{I}\right] + \boldsymbol{R}_\mu, \tag{7}$$

where p and μ are the fluid pressure and viscosity, respectively, and $\boldsymbol{I}$ is the identity tensor. A full description of the mathematical derivation can be found in our previous work (Capecelatro and Desjardins, 2013).

To account for the enhanced dissipation in the gas phase due to the presence of particles, an effective viscosity model is implemented, given by

$$\boldsymbol{R}_\mu \approx \mu^*[\nabla \boldsymbol{u}_f + \nabla \boldsymbol{u}_f^{\mathsf{T}} - \tfrac{2}{3}\ (\nabla \cdot \boldsymbol{u}_f)\boldsymbol{I}], \tag{8}$$

where μ^* was derived by Gibilaro et al. (2007) for fluidized beds as

$$\mu^* = \mu\left(\varepsilon_f^{-2.8} - 1\right). \tag{9}$$

As a result of filtering the non-linear convective term in the pointwise Navier–Stokes equation, a subfilter flux similar to the classical Reynolds stress term, $\boldsymbol{R}_u$, arises in Eq. (6). The isotropic components of $\boldsymbol{R}_u$ are absorbed into a modified mean pressure while the anisotropic part is modeled by an eddy viscosity model, given by

$$\boldsymbol{R}_u \approx \mu_t[\nabla \boldsymbol{u}_f + \nabla \boldsymbol{u}_f^{\mathsf{T}} - \tfrac{2}{3}\ (\nabla \cdot \boldsymbol{u}_f)\boldsymbol{I}], \tag{10}$$

where μ_t is similar to a turbulent viscosity, computed from a dynamic Smagorinsky model (Germano et al., 1991; Lilly, 1992) based on Lagrangian averaging (Meneveau et al., 1996). Note that the dynamic Smagorinsky model does not account for the presence of particles. Instead, μ^* is employed to account for any turbulence modulation generated at the scale of an individual particle, while the majority of the unsteady motion in the carrier-phase turbulence is assumed to be generated by clusters of particles with typical length scales that are sufficiently resolved by the computational mesh. We have observed in previous studies that both the effective viscosity and turbulent viscosity contribute very little to the total viscosity in moderately dilute gas-solid flows, and the majority of fluid-phase turbulent kinetic energy is produced by resolved wakes past clusters (Capecelatro et al., 2014a). A detailed study on cluster-induced turbulence in a non-reactive homogeneous riser can be found in our previous work (Capecelatro et al., 2014b).

2.3. Catalytic particle description

The solid phase is treated in a Lagrangian framework, where individual particle trajectories are solved using Newton's second law of motion. For each particle, its position $\boldsymbol{x}_p$, velocity $\boldsymbol{u}_p$, and angular velocity $\boldsymbol{\omega}_p$ are solved using a second-order Runge–Kutta scheme. The equations of motion for the particles are given by

$$\frac{d\boldsymbol{x}_p}{dt} = \boldsymbol{u}_p, \tag{11}$$

$$m_p \frac{d\boldsymbol{u}_p}{dt} = \boldsymbol{f}_p^{\text{inter}} + \boldsymbol{F}_p^{\text{col}} + m_p \boldsymbol{g}, \tag{12}$$

and

$$I_p \frac{d\boldsymbol{\omega}_p}{dt} = \sum_{j \neq p} \frac{d_p}{2} \boldsymbol{n} \times \boldsymbol{f}_{t,j\to p}^{\text{col}}, \tag{13}$$

where $m_p = \pi \rho_p d_p^3/6$ is the mass of particle p and $I_p = m_p d_p^2/10$ is the moment of inertia of the particle. In Eq. (12), $\boldsymbol{f}_p^{\text{inter}}$ is the force particle p experiences from the carrier fluid, and $\boldsymbol{F}_p^{\text{col}}$ is the collisional force that particle p experiences with adjacent particles and the walls. Particle rotation is assumed to be only a function of the tangential component of particle collisions $\boldsymbol{f}_t^{\text{col}}$, and aids in the contribution of tangential friction during contact. Collisions are handled via a soft-sphere approach based on the combination of a nonlinear Hertzian spring model combined with a dampening model for the normal component $\boldsymbol{f}_n^{\text{col}}$ (Cundall and Strack, 1979), and Coulomb friction law is applied for the tangential component $\boldsymbol{f}_t^{\text{col}}$. The model parameters are functions of the coefficient of restitution $0 < e < 1$, and a collision time that is a function of the simulation time step. To properly resolve the collisions without requiring an excessively small timestep, particles are restricted to

move no more than one-tenth of their diameter per timestep, and the collision time is set to 15 times the simulation timestep. Once each individual collision force is computed, the full collision force that particle p experiences can be expressed as a sum of collisions with all other particles j undergoing collision with p, i.e.,

$$\boldsymbol{F}_p^{\mathrm{col}} = \sum_{j \neq p} \left(\boldsymbol{f}_{n,j\to p}^{\mathrm{col}} + \boldsymbol{f}_{t,j\to p}^{\mathrm{col}} \right). \tag{14}$$

2.4. Interphase coupling

Coupling between the gas phase and solid particles appears in the form of the volume fraction ε_f, and interphase exchange term $\boldsymbol{F}^{\mathrm{inter}}$ defined by Eq. (16). Because the solid particles act as catalysts in the depletion of the chemical reactants, an accurate representation of the particle information on the Eulerian grid is crucial for predicting conversion rates. The particle-phase volume fraction and momentum exchange term can be expressed as

$$\varepsilon_p = 1-\varepsilon_f \approx \sum_{p=1}^{N_p} G(|\boldsymbol{x}-\boldsymbol{x}_p|)V_p, \tag{15}$$

and

$$\boldsymbol{F}^{\mathrm{inter}} \approx \sum_{p=1}^{N_p} G\left(|\boldsymbol{x}-\boldsymbol{x}_p|\right)\boldsymbol{f}_p^{\mathrm{inter}}, \tag{16}$$

where $\boldsymbol{f}_p^{\mathrm{inter}}$ is given by

$$\boldsymbol{f}_p^{\mathrm{inter}} \approx V_p \nabla\cdot\boldsymbol{\tau} + \boldsymbol{f}_p^{\mathrm{drag}} + \boldsymbol{F}^{\mathrm{mfr}}. \tag{17}$$

Details on the formulation can be found in Capecelatro and Desjardins (2013). The first term on the right-hand side of Eq. (16) represents contributions from the resolved fluid stresses that each particle experiences, and the second term accounts for the subfiltered stresses in the form of drag that relies on the gas-phase velocity and volume fraction. For statistically stationary flows, the forcing term $\boldsymbol{F}^{\mathrm{mfr}}$ acts as an effective pressure gradient on the particles. The gas-phase variables are interpolated to the location of the particle via a second order trilinear interpolation scheme and are used in the computation of the drag force by

$$\frac{\boldsymbol{f}_p^{\mathrm{drag}}}{m_p} = \frac{\varepsilon_f}{\tau_p}(\boldsymbol{u}_f-\boldsymbol{u}_p)F(\varepsilon_f,\mathrm{Re}_p), \tag{18}$$

where $\tau_p = \rho_p d_p^2/(18\mu)$ is the particle response time derived from Stokes flow and the particle Reynolds number is given by

$$\mathrm{Re}_p = \frac{\varepsilon_f\rho_f|\boldsymbol{u}_f-\boldsymbol{u}_p|d_p}{\mu}. \tag{19}$$

F is the dimensionless drag force coefficient of Tenneti et al. (2011), expressed as

$$F(\varepsilon_f,\mathrm{Re}_p) = \frac{1+0.15\mathrm{Re}_p^{0.687}}{\varepsilon_f^2} + \varepsilon_f F_1(\varepsilon_f) + \varepsilon_f F_2(\varepsilon_f,\mathrm{Re}_p), \tag{20}$$

where

$$F_1(\varepsilon_f) = \frac{5.81\varepsilon_p}{\varepsilon_f^3} + \frac{0.48\varepsilon_p^{1/3}}{\varepsilon_f^4},$$

and

$$F_2(\varepsilon_f,\mathrm{Re}_p) = \varepsilon_p^3\mathrm{Re}_p\left(0.95+\frac{0.61\varepsilon_p^3}{\varepsilon_f^2}\right).$$

To extrapolate the particle data back to the Eulerian mesh in a computationally efficient manner that is consistent with the mathematical formulation, Eqs. (15) and (16) are solved in two steps. First, the particle data is transferred to the nearest neighboring cells via linear extrapolation. The data is then diffused such that the final width of the filtering kernel is independent of the mesh size. In this work, G is taken to be Gaussian with a characteristic length scale $\delta_f = 8d_p$, defined as the full width at half the height of the kernel. To keep the cost low and ensure unconditional stability, the diffusion process is solved in a single implicit step by utilizing the approximate factorization scheme of Briley and McDonald (1977).

2.5. Discretization of the volume-filtered equations

The volume-filtered variable density equations are implemented in the framework of NGA (Desjardins et al., 2008), a high-order, fully conservative CFD code tailored for turbulent flow computations. The Navier–Stokes equations are solved on a staggered grid with second order spatial accuracy for both the convective and viscous terms, and the second order accurate semi-implicit Crank–Nicolson scheme of Pierce (2001) is implemented for time advancement. In this approach, the particles are advanced first, the scalar field is updated, and the momentum equations are then advanced. Scalar transport is solved via a bounded quadratic-upwind interpolative convective BQUICK scheme (Herrmann et al., 2006). Details on the mass, momentum, and energy conserving finite difference scheme are available in Desjardins et al. (2008).

This study considers gas-solid suspensions in vertical risers, where the reactor geometry is modeled as a vertical pipe with periodic boundary conditions imposed in the vertical (gravity-aligned) direction. To account for the cylindrical geometry on a cartesian mesh, a conservative immersed boundary (IB) method is employed. The IB method is based on a cut-cell formulation that requires rescaling of the convective and viscous fluxes in these cells, and exhibits formally second-order accuracy (Meyer et al., 2010; Desjardins et al., 2014). Details on the coupling of the Lagrangian particles with the IB method is provided in Capecelatro and Desjardins (2013).

3. Heterogeneous reactions in a three-dimensional riser

3.1. System description

In this study, reactive gas-solid flows take place in a vertical (i.e., gravity-aligned) cylindrical pipe with an aspect ratio of 10, on a cartesian mesh with $800\times82\times82$ cells and a uniform grid spacing of $\Delta x \approx 1.8d_p$. The density ratio and reactor diameter D to particle diameter ratio are respectively given by $\rho_p/\rho_f = 2500$ and $D/d_p = 150$. The particles are inelastic with a coefficient of restitution $e=0.9$ and coefficient of friction $\mu_f = 0.1$, initially uniformly distributed on a cartesian lattice with a mean concentration $\langle\varepsilon_p\rangle = 0.015$, corresponding to 728,232 particles. In this work, angled brackets denote a spatial average, i.e., $\langle(\cdot)\rangle = (1/V)\int_V (\cdot)\,dV$, with V being the volume of the system under consideration. Periodic boundary conditions are enforced in the streamwise direction and the momentum source term $\boldsymbol{F}^{\mathrm{mfr}}$ is adjusted dynamically in Eq. (6) to prevent the development of a net mass flow rate in the gas phase due to momentum coupling with the particles.

Once the flow reaches a statistically stationary state, a chemical reactant is introduced with a mass fraction of unity throughout and a Schmidt number $\mathrm{Sc} = \mu/(\rho_f\mathcal{D}) = 0.7$. The simulations are then run until 99% of the reactant is consumed. Note that both ρ_f and $\mathcal{D}$ remain constant throughout the duration of the simulations, and the chemistry does not modify the flow. The reaction rate k is varied in each simulation in order to emphasize the relative importance of the two-phase dynamics contributing to the chemical conversion process. These effects are quantified by the Damköhler number, Da, which describes the ratio of the flow

time scale to reaction time scale. Because the net mass flow rate is forced to zero, an appropriate timescale for the fluid is not obvious. We have shown in a previous numerical study (Capecelatro et al., 2014a) that clusters simulated in vertical risers fall with a constant velocity predicted by the experimental correlation of Noymer and Glicksman (2000), given by

$$U_c = 0.75\sqrt{\frac{\rho_p}{\rho_f} g d_p}. \tag{21}$$

Using Eq. (21) as the characteristic flow velocity and the reactor diameter D as the characteristic length scale for the flow, the Damköhler number can be formulated as

$$\mathrm{Da} = \frac{\langle \varepsilon_p \rangle k D}{\varepsilon_{p,0} U_c}, \tag{22}$$

where $\varepsilon_{p,0}/(\langle \varepsilon_p \rangle k)$ is the characteristic reaction time scale.

A total of 9 simulations are conducted by varying both Da and the Archimedes number Ar, which characterizes the entrainment of the gas phase by the particles (Goossens, 1998), defined as

$$\mathrm{Ar} = \frac{\left(\rho_p - \rho_f\right)\rho_f d_p^3 g}{\mu^2}. \tag{23}$$

A list of parameters for the simulations conducted in this work is shown in Table 1. The Archimedes number is varied by varying the gas-phase viscosity while keeping all other parameters constant. As a consequence, the particle response time τ_p, and thus the terminal velocity $v_t = \tau_p g$ increase with Ar. Because the cluster fall velocity is independent of Ar, U_c remains constant for each case. Furthermore, the Schmidt number is kept constant for each case, and therefore the species diffusivity decreases with increasing Ar.

Table 1
Simulation cases and their corresponding non-dimensional parameters.

Name	A_1	A_2	A_3	B_1	B_2	B_3	C_1	C_2	C_3
Ar	500	500	500	2500	2500	2500	12,500	12,500	12,500
Da	0.1	1.0	10.0	0.1	1.0	10.0	0.1	1.0	10.0

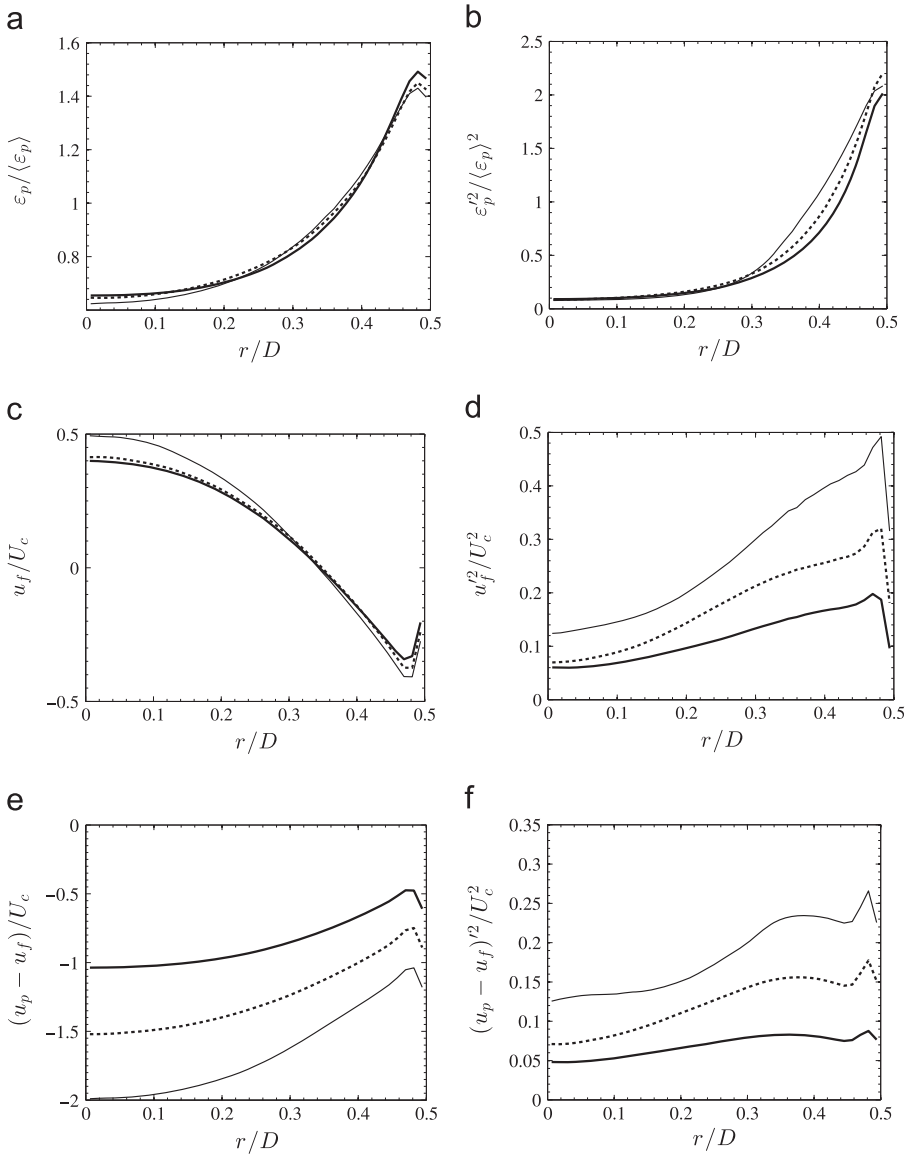

Fig. 1. Radial profiles extracted from Ar500 (thick solid line), Ar2500 (thick dashed line), and Ar12500 (thin solid line).

3.2. Gas-solid statistics

Simulation results are gathered after the initial transient is complete and the flow reaches a statistically stationary state. Time-averaged radial profiles of the multiphase statistics are shown in Fig. 1, where the single-prime notation denotes a fluctuation about the averaged quantity. It can be observed that the volume fraction statistics do not vary significantly with Ar. As seen in Fig. 1(a), the average solid concentration in the near-wall region is more than twice as large in comparison with the concentration in the center of the riser. Fluctuations in solid volume fraction along the radius of the pipe are given in Fig. 1(b), showing the greatest variation at the wall. The mean fluid velocity and fluctuations in fluid velocity increase monotonically with increasing Ar, as shown in Fig. 1(c) and (d). From the slip velocity profiles in Fig. 1(e) and (f), it is observed that the clusters in the near-wall region entrain the fluid, leading to a reduction in drag between the phases, and explaining the strong downward flow of gas closest to the walls. A more detailed analysis on the two-phase dynamics in risers can be found in our previous work (Capecelatro et al., 2014a).

3.3. Temporal evolution of reactant mass fraction in three dimensions

After the initial transient is complete, the chemical reactant is introduced to the flow with a mass fraction of unity. Fig. 2 shows two-dimensional planes colored by the spatial distribution of species mass fraction as a function of time from case B_2. Due to the strong segregation in particle concentration, the mass fraction decays rapidly in dense clusters, while maximum values of Y persist upstream of clusters and in the reactor center. The temporal evolution of the corresponding species mass fraction is shown in Fig. 3. After $tU_c/D \approx 6$, 99% of the overall chemical reactant has been depleted. The instantaneous minimum and maximum values of Y reveal the variation in local depletion times, with 99% consumption of reactant mass fraction occurring

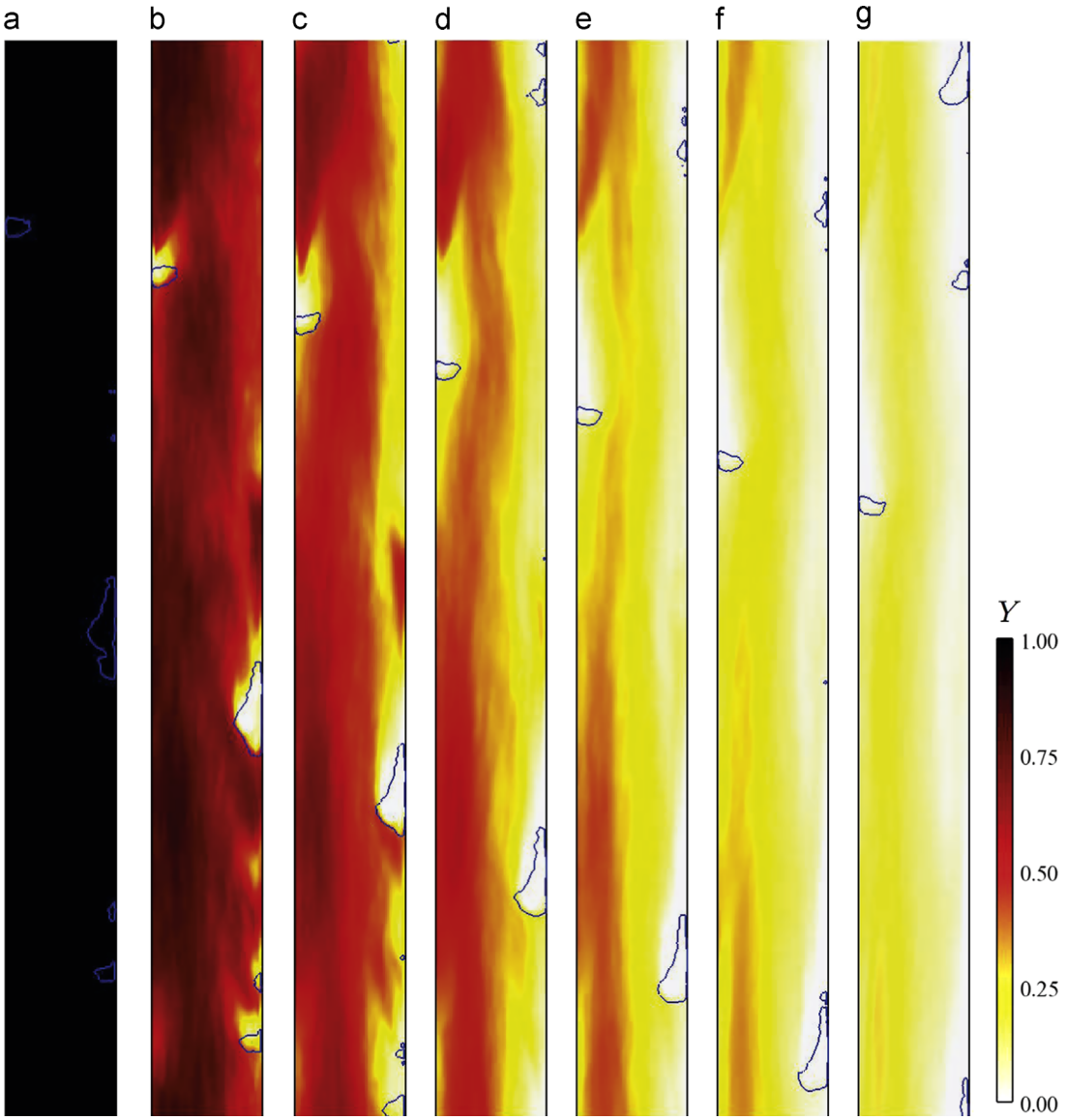

Fig. 2. Two-dimensional planes showing the spatial distribution of species mass fraction as a function of time for case B_2. Iso-contours of $\varepsilon_p = 3\langle\varepsilon_p\rangle$. (a) $tU_c/D = 0.0$, (b) $tU_c/D = 0.5$, (c) $tU_c/D = 1.0$, (d) $tU_c/D = 1.5$, (e) $tU_c/D = 2.0$, (f) $tU_c/D = 2.5$, and (g) $tU_c/D = 3.0$.

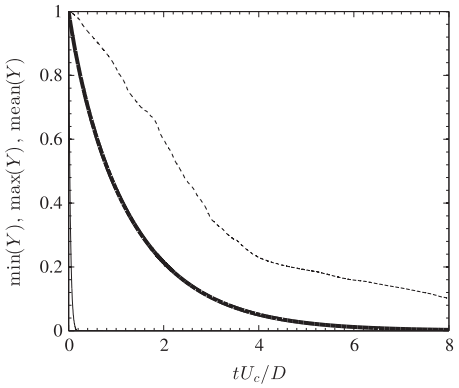

Fig. 3. Temporal evolution of the species mass fraction for case B_2. Phase-average mass fraction (thick solid line), minimum mass fraction (thin solid line), and maximum mass fraction (thin dashed line).

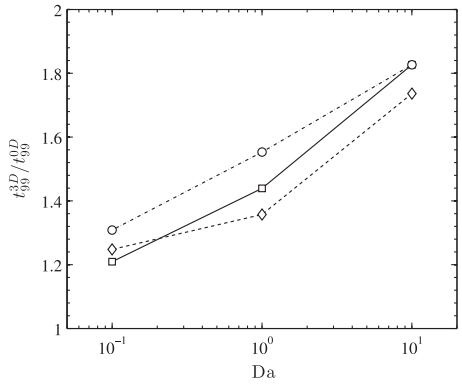

Fig. 4. Time until 99% of reactants are depleted, normalized by the value predicted by homogeneous solution Eq. (25) with Ar=500 (circles) Ar=2500 (diamonds), and Ar=12,500 (squares).

between $tU_c/D \approx 0.2$ in some regions of the flow and approximately $tU_c/D \approx 100$ in other regions.

4. Reduced-order modeling

4.1. Influence of clusters on the conversion time

Particle clustering is inherently a three-dimensional process characterized by strong lateral segregation in wall-bounded flows. To assess the effects of clustering on the catalytic-like conversion process, results from the three-dimensional simulations are compared to a zero-dimensional model that solves for the temporal evolution of the volume-averaged mass fraction and ignores all spatial variations. Applying the spatial averaging operator $\langle(\cdot)\rangle = (1/V_f)\int_{V_f}(\cdot)\,dV_f$ on the three-dimensional scalar transport, Eq. (3), yields

$$\frac{\partial \widetilde{Y}}{\partial t} + \frac{k\widetilde{\varepsilon}_p}{\varepsilon_{p,0}}\widetilde{Y} = -\frac{k}{\varepsilon_{p,0}}\widetilde{\varepsilon_p''Y''}, \tag{24}$$

where we have introduced the phase-average notation $\widetilde{(\cdot)} = \langle(\cdot)\varepsilon_f\rangle/\langle\varepsilon_f\rangle$ analogous to the Favre average in variable density flows, with double primes denoting a fluctuation about the volume fraction-weighted quantity, i.e. $(\cdot)'' = (\cdot) - \widetilde{(\cdot)}$. The unclosed term $\widetilde{\varepsilon_p''Y''}$ arises from averaging the chemical source term and accounts for fluctuations due to clustering. The homogeneous solution to Eq. (24) is given by

$$\widetilde{Y}(t) = e^{-t/\tau}, \tag{25}$$

where $\tau = \varepsilon_{p,0}/(k\widetilde{\varepsilon}_p)$ is the mean reaction timescale. The solution provided in Eq. (25) yields the temporal evolution of mass fraction given a homogeneous distribution of particles, and thus its deviation from the three-dimensional simulation is explicitly due to the presence of clusters.

The three-dimensional simulations listed in Table 1 are compared to the zero-dimensional solution given by Eq. (24) using the corresponding mean reaction timescale τ from each case. To assess the performance of the conversion process, the time required to deplete 99% of the reactants predicted by the three-dimensional simulation, t_{99}^{3D}, is compared with the depletion time predicted by the zero-dimensional solution, t_{99}^{0D}. Fig. 4 shows the effect of Da and Ar on the conversion times for each case. The deviation from the homogeneous solution is observed to increase with increasing Damköhler number, with a maximum of $t_{99}^{3D}/t_{99}^{0D} \approx 1.83$ for Da=10. At large values of Da, the reaction is relatively fast compared to the multiphase flow timescale, too fast for convection and diffusion to aid in the mixing process. Meanwhile, the Archimedes number is observed to have a small impact on the conversion rate.

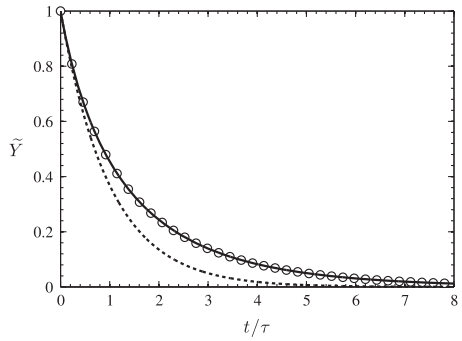

Fig. 5. Temporal evolution of the species mass fraction for case A_3. Phase-average mass fraction (thick solid line), homogeneous solution Eq. (25) (thick dashed line), and zero-dimensional model including the fluctuating source term Eq. (24) (circles).

The discrepancies between the simulation predictions and the homogeneous solutions are accounted for by the fluctuating chemical source term, $\widetilde{\varepsilon_p''Y''}$. In Fig. 5, the temporal evolution of the phase-average mass fraction predicted by case A_3 (maximum $t_{\text{res}}^{3D}/t_{\text{res}}^{0D}$) is compared to the corresponding zero-dimensional solutions with and without the fluctuating chemical source term, revealing that an accurate prediction of $\widetilde{\varepsilon_p''Y''}$ is critical when modeling reactive gas-solid flows that exhibit strong spatial segregation in particle concentration. The fluctuating source terms extracted from each simulation are shown in Fig. 6. For each case, $\widetilde{\varepsilon_p''Y''}$ peaks at approximately $t/\tau \approx 1$, corresponding to the time of maximum decay rate. Due to the non-passive and stochastic nature of the particle-phase volume fraction and its strong coupling with the species mass fraction, modeling $\widetilde{\varepsilon_p''Y''}$ requires careful attention.

4.2. Transport of the fluctuating chemical source term

A transport equation for the fluctuating chemical source can be derived by subtracting Eq. (24) from Eq. (3) and multiplying through by ε_p'', yielding the following differential equation

$$\frac{\partial}{\partial t}\widetilde{\varepsilon_p''Y''} + \frac{k\widetilde{\varepsilon}_p}{\varepsilon_{p,0}}\widetilde{\varepsilon_p''Y''} = Y\widetilde{\boldsymbol{u}_f\cdot\nabla\varepsilon_p''} + \mathcal{D}\widetilde{\varepsilon_p''\nabla^2 Y''} - \frac{k}{\varepsilon_{p,0}}\left(\widetilde{\varepsilon_p''^2}\widetilde{Y} + \widetilde{\varepsilon_p''^2 Y''}\right) + Y''\widetilde{\frac{\partial\varepsilon_p''}{\partial t}}. \tag{26}$$

It is important to recall that the phase-average quantities involve volume averaging over the entire domain, and thus mean gradients are not retained. The first two terms on the right-hand side of

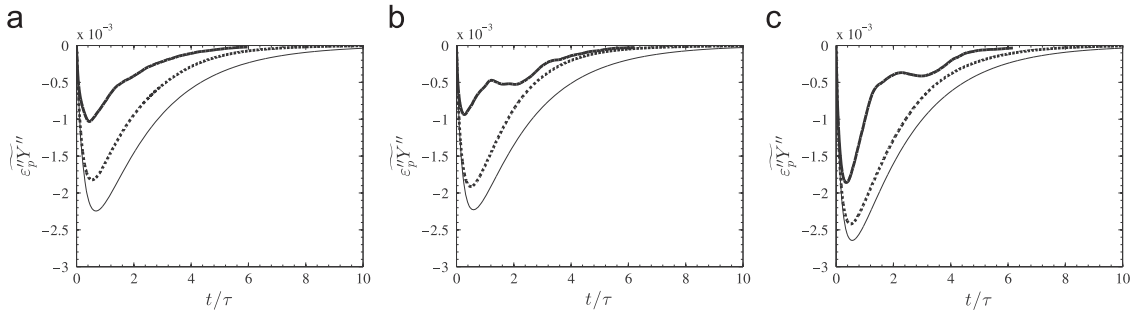

Fig. 6. Fluctuating chemical source term extracted from the three-dimensional simulations with Da = 0.1 (thick solid line), Da = 1.0 (thick dashed line), and Da = 10 (thin solid line): (a) Ar=500; (b) Ar=2500; and (c) Ar=12,500.

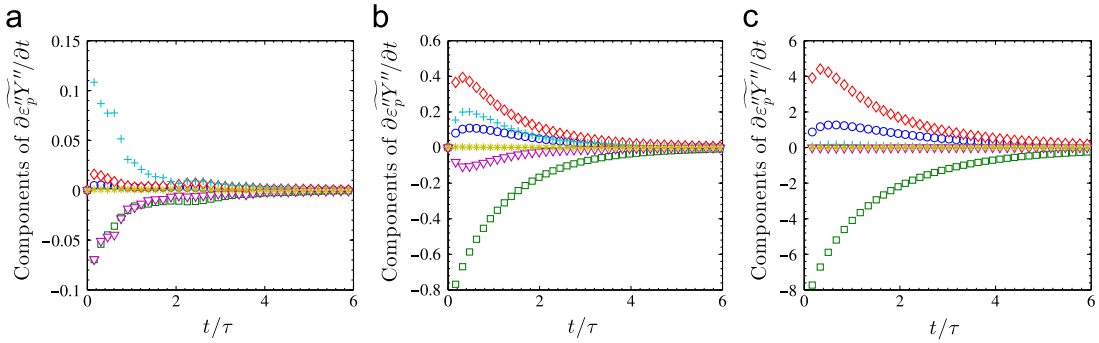

Fig. 7. Components of the fluctuating chemical source term Eq. (26) for Ar=2500. $-k/\varepsilon_{p,0}\widetilde{\varepsilon}_p\widetilde{\varepsilon_p''Y''}$ (blue circles), $\widetilde{Y\boldsymbol{u}_f\cdot\nabla\varepsilon_p''}$ (pink triangles), $\widetilde{\mathcal{D}\varepsilon_p''\nabla^2 Y''}$ (yellow stars), $-k/\varepsilon_{p,0}\widetilde{Y}\widetilde{\varepsilon_p''^2}$ (green squares), $-k/\varepsilon_{p,0}\widetilde{\varepsilon_p''^2Y''}$ (red diamonds), and $\widetilde{Y''\partial\varepsilon_p''/\partial t}$ (blue crosses): (a) Case B_1; (b) Case B_2; and (c) Case B_3. (For interpretation of the references to color in this figure caption, the reader is referred to the web version of this article.)

this equation represent sources due to convection and diffusion, respectively. The third and fourth terms account for fluctuations in particle-phase volume fraction. The last term is a correlation between mass fraction fluctuations and the rate of change of volume fraction fluctuations. The relative contributions from each term in Eq. (26) are provided in Fig. 7. For each case, the diffusive flux is observed to have a negligible contribution, while all other terms contribute to the fluctuating chemical source term in various degrees. When the chemical reaction is sufficiently fast (i.e., Da=10), convection is seen to have very little influence, but when reactions take place over longer timescales (i.e., smaller Da), the relative importance of convection is higher. Similarly, $\widetilde{Y''\partial\varepsilon_p''/\partial t}$ decreases with increasing Da, but with a positive contribution and thus this term inhibits the overall conversion rate. For each case, $-k/\varepsilon_{p,0}\widetilde{Y}\widetilde{\varepsilon_p''^2}$ has the greatest contribution to the fluctuating chemical source term, and is observed to promote the conversion of species mass fraction, while $-k/\varepsilon_{p,0}\widetilde{\varepsilon_p''^2Y''}$ also has a significant impact for each case, but reduces the overall conversion rate.

We have demonstrated in our previous work that the empirical model of Issangya et al. (2000) provides reasonable agreement with the volume fraction variance for a wide range of Ar (Capecelatro et al., 2014a). This model can be written in terms of the phase-average concentration as

$$\widetilde{\varepsilon_p''^2} = \left[1.584\widetilde{\varepsilon}_p(0.55-\widetilde{\varepsilon}_p)\right]^2. \tag{27}$$

This expression provides closure for the most significant contribution to the fluctuating chemical source term in Eq. (26). Note that a more accurate model for the volume fraction variance based on first-principles, as opposed to an empirical correlation, will be useful in the context of large-eddy simulations, and will require careful analysis of a canonical fluid-particle flow such as the case of fully developed cluster-induced turbulence recently introduced elsewhere (Capecelatro et al., 2014b). From Fig. 7, it is observed that $\widetilde{\varepsilon_p''^2Y''}$ varies like

$$\widetilde{\varepsilon_p''^2Y''} \approx C\widetilde{\varepsilon_p''Y''}\left(\widetilde{\varepsilon_p''^2}\right)^{1/2}, \tag{28}$$

where C is a modeling constant. In Fig. 8, Eqs. (27) and (28) are compared to results from each simulation case, showing overall good agreement. Meanwhile, for small values of Da, contributions from convection and the rate of change in volume fraction fluctuations in the transport of the fluctuating chemical source term become important. Providing models for all of the relevant terms (i.e., $-k/\varepsilon_{p,0}\widetilde{\varepsilon}_p\widetilde{\varepsilon_p''Y''}$, $\widetilde{Y\boldsymbol{u}_f\cdot\nabla\varepsilon_p''}$, $-k/\varepsilon_{p,0}\widetilde{Y}\widetilde{\varepsilon_p''^2}$, $-k/\varepsilon_{p,0}\widetilde{\varepsilon_p''^2Y''}$, and $\widetilde{Y''\partial\varepsilon_p''/\partial t}$) becomes challenging, and alternative modeling approaches should be explored.

4.3. Presumed shape PDF approach

The fluctuating chemical source term can be calculated provided the density field is known, i.e.,

$$\widetilde{\varepsilon_p''Y''} = \int\int(\varepsilon_p-\widetilde{\varepsilon}_p)(Y-\widetilde{Y})\widetilde{f}(\varepsilon_p,Y)\,d\varepsilon_p\,dY, \tag{29}$$

where $\widetilde{f}(\varepsilon_p,Y)$ is the phase-average joint-PDF, given by

$$\widetilde{f}(\varepsilon_p,Y) = \frac{\langle\varepsilon_f|\varepsilon_p,Y\rangle}{\langle\varepsilon_f\rangle}f(\varepsilon_p,Y), \tag{30}$$

with $f(\varepsilon_p,Y)$ the joint-PDF of particle volume fraction and species mass fraction. The temporal evolution of the phase-average joint-PDF is given in Fig. 9 for case B_2. Because the gas-solid flow is at steady state and there is no feedback from the chemical species, the mean volume fraction remains constant throughout the duration of the simulation. Meanwhile, the phase-average species mass fraction is strongly coupled with both particle concentration and time. Making use of Bayes' theorem, the joint-PDF can be

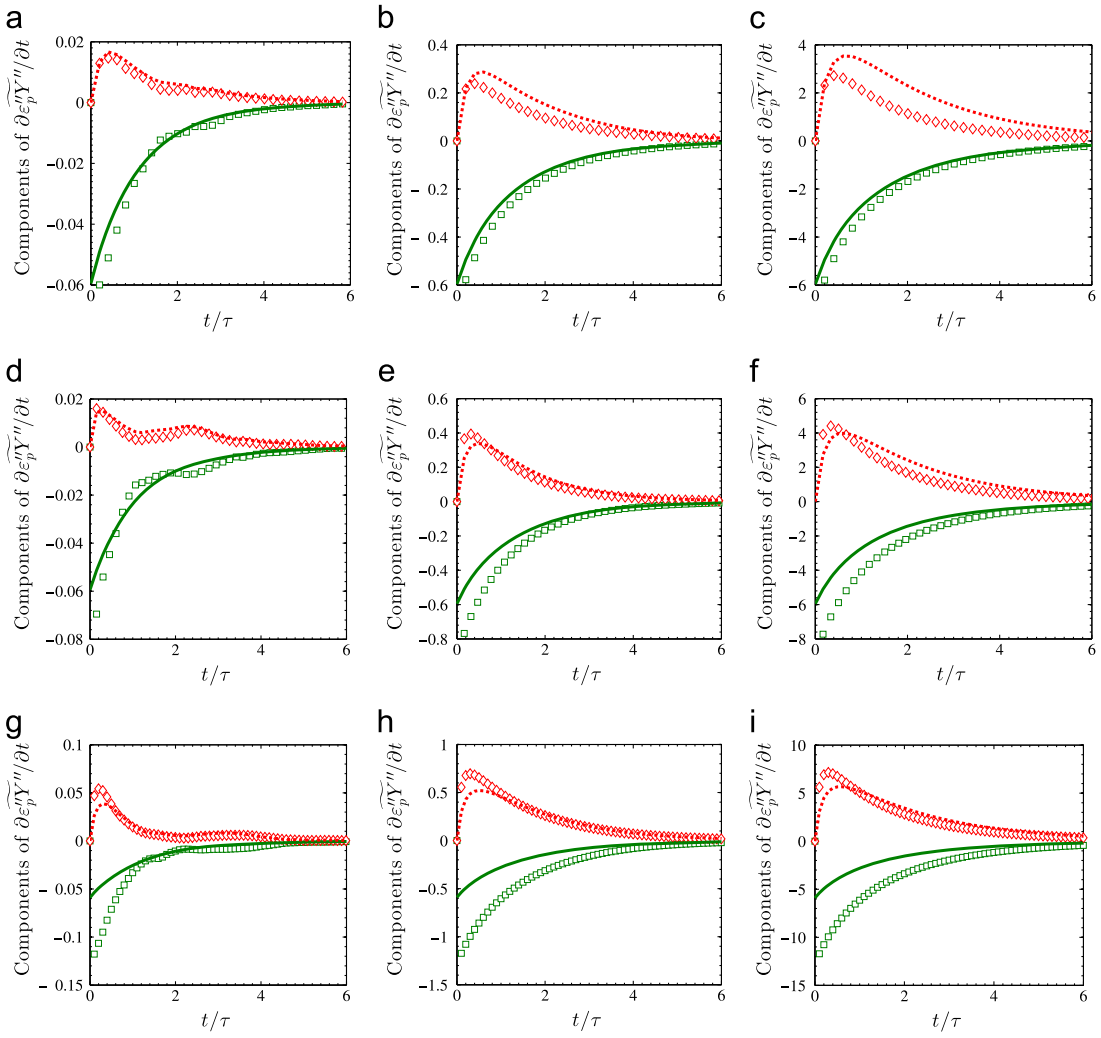

Fig. 8. Models for selected components of the fluctuating chemical source term (lines) against simulation results (symbols). $-k/\varepsilon_{p,0}\widetilde{Y}\widetilde{\varepsilon_p''^2}$ (green squares), variance modeled using Eq. (27) (green line), $-k/\varepsilon_{p,0}\widetilde{\varepsilon_p''^2}\widetilde{Y''}$ (red diamonds), Eq. (28) with $C=3$ (red dashed-line): (a) Case A_1; (b) Case A_2; (c) Case A_3; (d) Case B_1; (e) Case B_2; (f) Case B_3; (g) Case C_1; (h) Case C_2; and (i) Case C_3. (For interpretation of the references to color in this figure caption, the reader is referred to the web version of this article.)

rewritten as

$$\widetilde{f}(\varepsilon_p, Y) = \widetilde{f}(Y|\varepsilon_p)\widetilde{g}(\varepsilon_p), \tag{31}$$

where the conditional PDF $\widetilde{f}(Y|\varepsilon_p)$ and volume fraction PDF $\widetilde{g}(\varepsilon_p)$ may be modeled based on a presumed distribution.

4.3.1. Modeling the volume fraction PDF

We have demonstrated in our previous work that the PDF of particle-phase volume fraction in CFB risers closely resembles a lognormal distribution for a wide range of Ar (Capecelatro et al., 2014a). Using the instantaneous phase-average concentration $\widetilde{\varepsilon}_p$ and making use of Eq. (27), the volume fraction PDF can be modeled as

$$\widetilde{g}(\varepsilon_p) = \frac{1}{\varepsilon_p \sigma_{\ln}\sqrt{2\pi}} \exp\left[-\frac{(\ln \varepsilon_p - \mu_{\ln})^2}{2\sigma_{\ln}^2}\right], \tag{32}$$

where $\mu_{\ln} = \ln\left[\widetilde{\varepsilon}_p^2/\left(\widetilde{\varepsilon_p''^2}+\widetilde{\varepsilon}_p^2\right)^{1/2}\right]$ and $\sigma_{\ln} = \left[\ln\left(1+\widetilde{\varepsilon_p''^2}/\widetilde{\varepsilon}_p\right)\right]^{1/2}$. A comparison between $\widetilde{g}(\varepsilon_p)$ extracted from the simulations with the corresponding lognormal distribution using the model of Issangya et al. (2000) for the variance is given in Fig. 10, showing overall very good agreement.

4.3.2. Modeling the conditional PDF

In non-premixed combustion, the beta PDF has been used in numerous studies to model the scalar mass fraction in both constant and variable-density flows with much success (see e.g., Cook and Riley, 1994; Jiménez et al., 1997; Wall et al., 2000; Tong, 2001; Pierce and Moin, 2004). Recent studies suggest that the beta distribution is also capable of capturing mixing of active scalars in variable-density, buoyancy-driven (or other pressure-gradient-driven) turbulence (Bakosi and Ristorcelli, 2010). However, it remains unclear whether such an approach can be applied to reactive particle-laden flows.

Assuming the species mass fraction is well represented by a beta distribution, the conditional PDF can be written in terms of two parameters a and b as

$$\widetilde{f}(Y|\varepsilon_p) = \frac{(Y|\varepsilon_p)^{a-1}(1-Y|\varepsilon_p)^{b-1}}{B(a,b)}, \tag{33}$$

which is bounded by $0 \le Y \le 1$. In Eq. (33), $B(a,b)$ is a normalization constant to ensure $\widetilde{f}(Y|\varepsilon_p)$ integrates to unity, given by the beta function

$$B(a,b) = \int_0^1 y^{a-1}(1-y)^{b-1}\, dy. \tag{34}$$

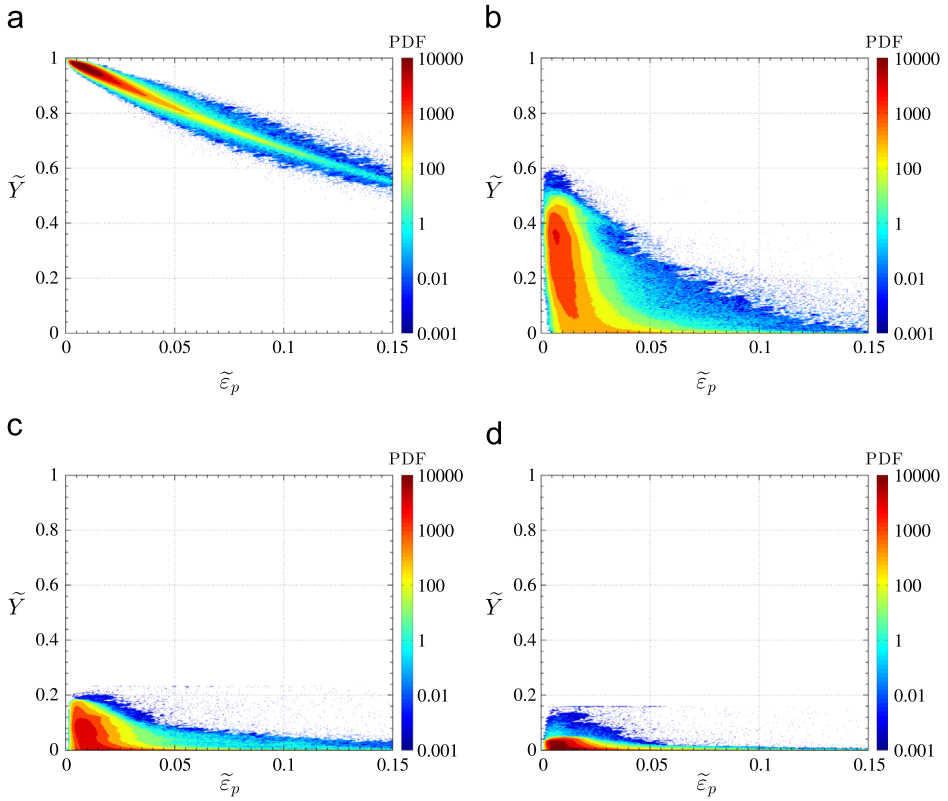

Fig. 9. Instantaneous phase-average joint-PDFs of particle concentration and species mass fraction for case B_2: (a) $t/\tau=0.1$; (b) $t/\tau=2.0$; (c) $t/\tau=4.0$; and (d) $t/\tau=6.0$.

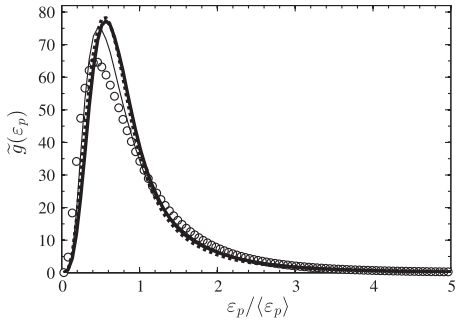

Fig. 10. Instantaneous phase-average PDF of particle concentration. Ar=500 (solid line), Ar=2500 (dashed line), Ar=12,500 (thin solid line), and the corresponding lognormal distribution (Eq. (32)) using the correlation provided by Issangya et al., 2000 for modeling the variance (circles).

The two parameters a and b are related to the conditional moments by

$$a=\widetilde{Y}|\varepsilon_p\left[\frac{\widetilde{Y}|\varepsilon_p(1-\widetilde{Y}|\varepsilon_p)}{\widetilde{Y''^2}|\varepsilon_p}-1\right], \tag{35}$$

and

$$b=(1-\widetilde{Y}|\varepsilon_p)a. \tag{36}$$

Using the conditional moments extracted from case B_2, Fig. 11 demonstrates the capability of the beta distribution to reproduce the conditional PDF, showing overall excellent agreement. Due to the conditional dependence on the volume fraction, the parameters a and b must be known for every value of ε_p at each time t. In the similar situation of non-premixed combustion problems, conditional moment closure (CMC) methods have been used to derive and model equations for the conditional moments of reactive scalars with encouraging success (Klimenko and Bilger, 1999). Modeling $\widetilde{Y}|\varepsilon_p$ and $\widetilde{Y''^2}|\varepsilon_p$ with CMC methods would require knowledge of the fluid velocity and scalar dissipation conditioned on the particle-phase volume fraction and is beyond the scope of this work.

4.3.3. *Validation of the presumed PDF strategy*

The fluctuating chemical source term that appears in the zero-dimensional scalar transport, Eq. (24), is closed via Eq. (29), where the phase-average joint-PDF is modeled as a product of a beta distribution for the conditional mass fraction and a lognormal distribution for the particle-phase volume fraction. The volume fraction variance is modeled using the correlation by Issangya et al. (2000), and the conditional moments are obtained from the three-dimensional simulations. Fig. 12 shows the modeled phase-average joint-PDF as a function of time for case B_2. The model shows excellent agreement with the joint-PDF predicted by the simulation in Fig. 9. Finally, Fig. 13 shows that the PDF model provides an excellent representation of the volume fraction-mass fraction correlation for the range of Da considered in this study.

5. Conclusions

The turbulent and multiphase nature of riser reactors will often lead to a strong segregation of the solid phase in the form of dense clusters. It is hypothesized that the non-homogeneity in particle concentration will affect the conversion process, rendering optimal operation difficult to achieve since a much higher catalyst loading will be necessary to obtain the desired level of conversion. The aim of this study was to investigate the effect of clusters on the conversion process and develop a reduced-order model that takes these effects into account. The choice of chemical model was driven by the objectives of simplicity and generality, such that the insights gained from this analysis remains applicable to a wide range of gas-solid catalytic processes. In order to formulate a

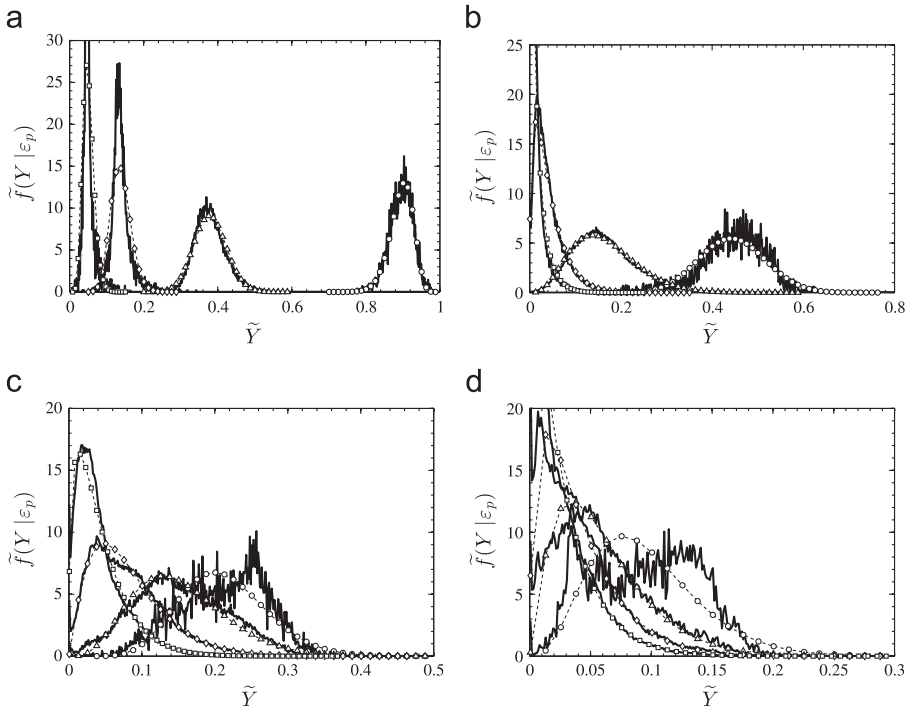

Fig. 11. Instantaneous conditional PDFs of species mass fraction from case B_1 (solid line) compared to their corresponding beta distributions (symbols) as a function of ε_p. (a) $\varepsilon_p = 0.001$ (circles), $\varepsilon_p = .025$ (triangles), $\varepsilon_p = 0.05$ (diamonds), $\varepsilon_p = 0.075$ (squares). (b) $\varepsilon_p = 0.001$ (circles), $\varepsilon_p = 0.01$ (triangles), $\varepsilon_p = 0.018$ (diamonds), $\varepsilon_p = 0.025$ (squares). (c) $\varepsilon_p = 0.001$ (circles), $\varepsilon_p = 0.003$ (triangles), $\varepsilon_p = 0.006$ (diamonds), $\varepsilon_p = 0.01$ (squares). (d) $\varepsilon_p = 0.001$ (circles), $\varepsilon_p = 0.003$ (triangles), $\varepsilon_p = 0.043$ (diamonds), and $\varepsilon_p = 0.006$ (squares).

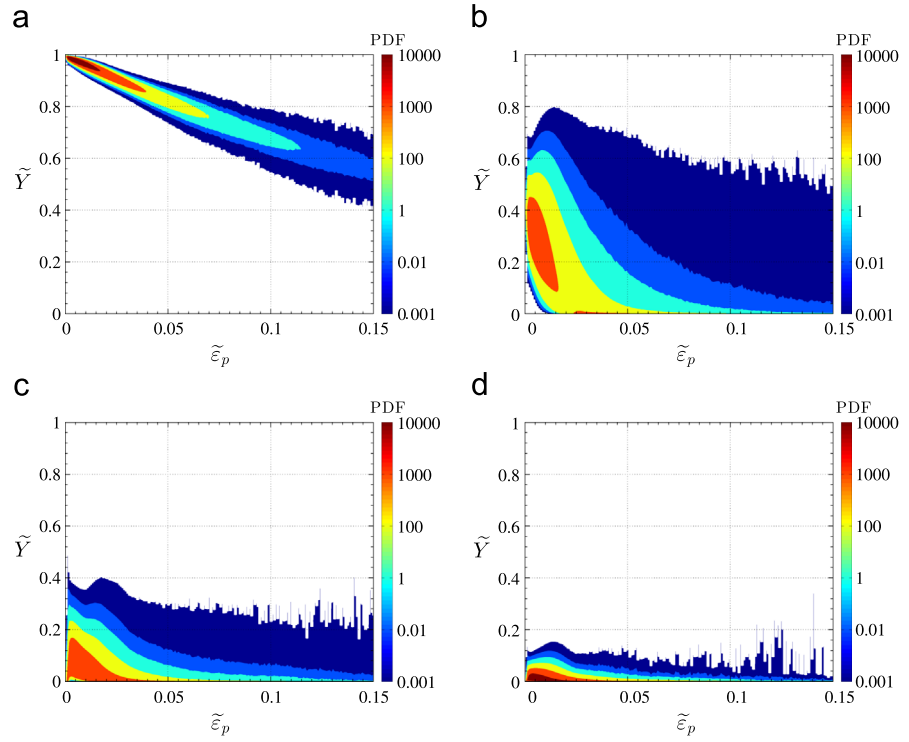

Fig. 12. Model of the instantaneous phase-average joint-PDFs for case B_2: (a) $t/\tau = 0.1$; (b) $t/\tau = 2.0$; (c) $t/\tau = 4.0$; and (d) $t/\tau = 6.0$.

tractable system of equations that accounts for key physical processes of the flow, a volume-filtering operator was applied to the microscale equations of motion. The equations were discretized in an Eulerian–Lagrangian framework and applied to flows of isothermal, linearly reacting chemical species in fully developed three-dimensional risers. The Archimedes number, Ar, was varied by a factor of 25, $500 \leq \mathrm{Ar} \leq 12,500$, and the Damköhler number, Da, by a factor of 100, $0.1 \leq \mathrm{Da} \leq 10$. Key findings from this work include:

- The PDF of particle-phase volume fraction in fully developed risers closely resembles a lognormal distribution with a concentration variance modeled using the correlation of Issangya et al. (2000).

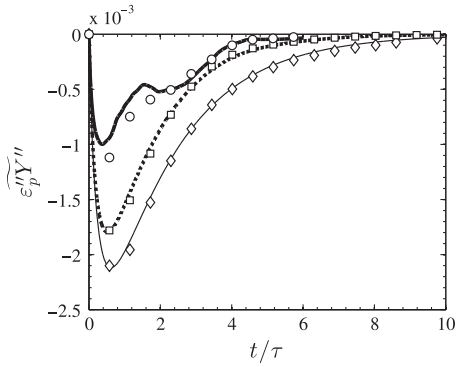

Fig. 13. Temporal evolution of $\widetilde{\varepsilon_p''Y''}$ for Ar = 2500 extracted from simulations (lines) and presumed-shape PDF model (symbols). Case B_1 (solid line) and corresponding model (circles), case B_2 (dashed line) and corresponding model (squares), and case B_3 (thin solid line) and corresponding model (diamonds).

- To assess the impact of clusters on the heterogeneous reaction, a zero-dimensional model that solves for the temporal evolution of the phase-average mass fraction was derived. The correlation between fluctuating mass fraction and volume fraction entirely accounts for the discrepancy between the zero-dimensional model and three-dimensional results.
- Clusters are found to delay the conversion process by up to 85% compared to the homogeneous solution, with greater impact at higher Da.
- A transport equation for the fluctuating chemical source term was derived, and the correlation of Issangya et al. (2000) was used to model the two largest contributions, showing overall very good agreement.
- An initial attempt at providing closure for the fluctuating chemical source term in the zero-dimensional model was obtained by applying a presumed-shape PDF model, where the phase-average joint-PDF is given by a product of a beta distribution for the species mass fraction and a lognormal distribution for the particle concentration. The model yields excellent results for the range of Ar and Da considered in this study.

In practice, riser reactors used in catalytic conversion contain both a population of deactivated catalysts that are trapped in clusters as well as freshly re-injected particles. In future studies, it would be necessary to account for deactivation of catalytic particles that have been exposed to chemical reactants for a sufficiently long period of time, which is likely to further reduce the conversion efficiency of the reactor, and further amplify the role played by clusters.

References

Agrawal, K., Loezos, P., Syamlal, M., Sundaresan, S., 2001. The role of meso-scale structures in rapid gas-solid flows. J. Fluid Mech. 445, 151–186.

Avidan, A.A., 1996. Fluid catalytic cracking. In: Circulating Fluidized Beds. Springer, Netherlands, pp. 466–488.

Avidan, A., Edwards, M., Owen, H., 1990. Fluid-catalytic cracking-past and future challenges. Rev. Chem. Eng. 6, 1–72.

Bakosi, J., Ristorcelli, R., 2010. Probability Density Function Method for Variable-Density Pressure-Gradient-Driven Turbulence and Mixing. Technical Report, Los Alamos National Laboratory (LANL).

Basu, P., 2006. Combustion and Gasification in Fluidized Beds. CRC Press, (Taylor & Francis Group), Boca Raton, FL, USA.

Desjardins, O., McCaslin, J., Owkes, M., Brady, P., 2014. Direct numerical and large-eddy simulation of primary atomization in complex geometries. Atomization and Sprays 23, 1001–1048, http://dx.doi.org/10.1615/AtomizSpr.2013007679.

Brereton, C., 1996. Combustion performance. In: Circulating Fluidized Beds. Springer, Netherlands, pp. 369–416.

Briley, W., McDonald, H., 1977. Solution of the multidimensional compressible Navier–Stokes equations by a generalized implicit method. J. Comp. Phys. 24, 372–397.

Bruchmüller, J., van Wachem, B., Gu, S., Luo, K., Brown, R., 2012. Modeling the thermochemical degradation of biomass inside a fast pyrolysis fluidized bed reactor. AIChE J. 58, 3030–3042.

Capecelatro, J., Desjardins, O., 2013. An Euler–Lagrange strategy for simulating particle-laden flows. J. Comp. Phys. 238, 1–31.

Capecelatro, J., Pepiot, P., Desjardins, O., 2014a. Numerical characterization and modeling of particle clustering in wall-bounded vertical risers. Chem. Eng. J. 245, 295–310.

Capecelatro, J., Desjardins, O., Fox, R.O., 2014b. Numerical study of collisional particle dynamics in cluster-induced turbulence. J. Fluid Mech. 747 (R2), 1–13.

Cook, A., Riley, J., 1994. A subgrid model for equilibrium chemistry in turbulent flows (1994-present). Phys. Fluids 6, 2868–2870.

Cundall, P., Strack, O., 1979. A discrete numerical model for granular assemblies. Geotechnique 29, 47–65.

Das, A., Baudrez, E., Marin, G., Heynderickx, G., 2003. Three-dimensional simulation of a fluid catalytic cracking riser reactor. Ind. Eng. Chem. Res. 42, 2602–2617.

Derksen, J., 2008. Scalar mixing by granular particles. AIChE J. 54, 1741–1747.

Derksen, J., 2014. Simulations of scalar dispersion in fluidized solid–liquid suspensions. AIChE J. 60 (5), 1880–1890 http://dx.doi.org/10.1002/aic.14372.

Derouin, C., Nevicato, D., Forissier, M., Wild, G., Bernard, J., 1997. Hydrodynamics of riser units and their impact on FCC operation. Ind. Eng. Chem. Res. 36, 4504–4515.

Desjardins, O., Blanquart, G., Balarac, G., Pitsch, H., 2008. High order conservative finite difference scheme for variable density low Mach number turbulent flows. J. Comput. Phys. 227, 7125–7159.

Fletcher, D., Haynes, B., Christo, F., Joseph, S., 2000. A CFD based combustion model of an entrained flow biomass gasifier. Appl. Math. Modell. 24, 165–182.

Germano, M., Piomelli, U., Moin, P., Cabot, W., 1991. A dynamic subgrid-scale eddy viscosity model. Phys. Fluids A: Fluid Dyn. 3, 1760.

Gibilaro, L., Gallucci, K., Di Felice, R., Pagliai, P., 2007. On the apparent viscosity of a fluidized bed. Chem. Eng. Sci. 62, 294–300.

Gidaspow, D., 1994. Multiphase Flow and Fluidization: Continuum and Kinetic Theory Descriptions. Academic Press, San Diego, California.

Goossens, W.R., 1998. Classification of fluidized particles by Archimedes number. Powder Technol. 98, 48–53.

Gupta, A., Subba Rao, D., 2001. Model for the performance of a fluid catalytic cracking (FCC) riser reactor: effect of feed atomization. Chem. Eng. Sci. 56, 4489–4503.

Herrmann, M., Blanquart, G., Raman, V., 2006. A bounded quick scheme for preserving scalar bounds in large-eddy simulations. AIAA J. 44, 2879–2880.

Issangya, A.S., Grace, J.R., Bai, D., Zhu, J., 2000. Further measurements of flow dynamics in a high-density circulating fluidized bed riser. Powder Technol. 111, 104–113.

Jiménez, J., Liñán, A., Rogers, M.M., Higuera, F.J., 1997. A priori testing of subgrid models for chemically reacting non-premixed turbulent shear flows. J. Fluid Mech. 349, 149–171.

Klimenko, A., Bilger, R., 1999. Conditional moment closure for turbulent combustion. Progr. Energy Combust. Sci. 25, 595–687.

Lee, Y.Y., 1996. Design considerations for CFB boilers. In: Circulating Fluidized Beds. Springer, Netherlands, pp. 417–440.

Li, X., Grace, J., Lim, C., Watkinson, A., Chen, H., Kim, J., 2004. Biomass gasification in a circulating fluidized bed. Biomass Bioenergy 26, 171–193.

Li, J., Luo, Z.-H., Lan, X.-Y., Xu, C.-M., Gao, J.-S., 2013. Numerical simulation of the turbulent gas–solid flow and reaction in a polydisperse FCC riser reactor. Powder Technol. 237, 569–580 http://dx.doi.org/10.1016/j.powtec.2012.12.062.

Li, T., Pannala, S., Shahnam, M., 2014. CFD simulations of circulating fluidized bed risers, Part II, evaluation of differences between 2D and 3D simulations. Powder Technol. 254, 115–124.

Lilly, D., 1992. A proposed modification of the germano subgrid-scale closure method. Phys. Fluids A: Fluid Dyn. 4, 633.

Meneveau, C., Lund, T., Cabot, W., 1996. A Lagrangian dynamic subgrid-scale model of turbulence. J. Fluid Mech. 319, 353–385.

Meyer, M., Devesa, A., Hickel, S., Hu, X., Adams, N., 2010. A conservative immersed interface method for Large-Eddy Simulation of incompressible flows. J. Comput. Phys. 229 (18), 6300–6317 http://dx.doi.org/10.1016/j.jcp.2010.04.040.

Noymer, P.D., Glicksman, L.R., 2000. Descent velocities of particle clusters at the wall of a circulating fluidized bed. Chem. Eng. Sci. 55, 5283–5289.

Oevermann, M., Gerber, S., Behrendt, F., 2009. Euler–Lagrange/DEM simulation of wood gasification in a bubbling fluidized bed reactor. Particuology 7, 307–316.

Ozel, A., Fede, P., Simonin, O., 2013. Development of filtered Euler–Euler two-phase model for circulating fluidised bed: high resolution simulation, formulation and a priori analyses. Int. J. Multiph. Flow 55, 43–63 http://dx.doi.org/10.1016/j.ijmultiphaseflow.2013.04.002.

Papadikis, K., Gu, S., Bridgwater, A.V., Gerhauser, H., 2009. Application of CFD to model fast pyrolysis of biomass. Fuel Process. Technol. 90, 504–512.

Peirano, E., Leckner, B., 1998. Fundamentals of turbulent gas-solid flows applied to circulating fluidized bed combustion. Progr. Energy Combust. Sci. 24, 259–296.

Pierce, C., 2001. Progress-variable Approach for Large-eddy Simulation of Turbulent Combustion (Ph.D. thesis), Citeseer.

Pierce, C.D., Moin, P., 2004. Progress-variable approach for large-eddy simulation of non-premixed turbulent combustion. J. Fluid Mech. 504, 73–97.

Prasad Vegendla, S., Heynderickx, G., Marin, G., 2012. Probability density function simulation of turbulent reactive gas-solid flow in a FCC riser. AIChE J. 58, 268–284.

Rabinovich, O., Borodulya, V., Vinogradov, L., Korban, V., 2010. Fast pyrolysis of an ensemble of biomass particles in a fluidized bed. J. Eng. Phys. Thermophys. 83, 742–752.
Sanz, A., Corella, J., 2006. Modeling circulating fluidized bed biomass gasifiers, results from a pseudo-rigorous 1-dimensional model for stationary state. Fuel Process. Technol. 87, 247–258.
Scott, G., Kilgour, D., 1969. The density of random close packing of spheres. J. Phys. D: Appl. Phys. 2, 863.
Shaffer, F., Gopalan, B., Breault, R.W., Cocco, R., Karri, S., Hays, R., Knowlton, T., 2013. High speed imaging of particle flow fields in CFB risers. Powder Technol 242, 86–99 http://dx.doi.org/10.1016/j.powtec.2013.01.012.
Souza, J., Vargas, J., Von Meien, O., Martignoni, W., Amico, S., 2006. A two-dimensional model for simulation, control, and optimization of FCC risers. AIChE J. 52, 1895–1905.
Speight, J., 2014. The Chemistry and Technology of Petroleum. CRC Press, Boca Raton, FL.
Szekely, J., Evans, J.W., Sohn, H., 1976. Gas-solid Reactions. Academic Press, New York.
Tenneti, S., Garg, R., Subramaniam, S., 2011. Drag law for monodisperse gas-solid systems using particle-resolved direct numerical simulation of flow past fixed assemblies of spheres. Int. J. Multiph. Flow 37, 1072–1092.
Theologos, K., Markatos, N., 1993. Advanced modeling of fluid catalytic cracking riser-type reactors. AIChE J. 39, 1007–1017.
Tong, C., 2001. Measurements of conserved scalar filtered density function in a turbulent jet. Phys. Fluids 13, 2923–2937.
Treece, G., Prager, R., Gee, A., 1999. Regularised marching tetrahedra: improved iso-surface extraction. Comput. Graph. 23, 583–598.
Wall, C., Boersma, B., Moin, P., 2000. An evaluation of the assumed beta probability density function subgrid-scale model for large eddy simulation of nonpre-mixed, turbulent combustion with heat release. Phys. Fluids 12, 2522–2529.
Wu, C., Cheng, Y., Jin, Y., 2008. Understanding riser and downer based fluid catalytic cracking processes by a comprehensive two-dimensional reactor model. Ind. Eng. Chem. Res. 48, 12–26.
Wu, C., Cheng, Y., Ding, Y., Jin, Y., 2010. CFD–DEM simulation of gas–solid reacting flows in fluid catalytic cracking (FCC) process. Chem. Eng. Sci. 65, 542–549.
Zhang, D., Prosperetti, A., 1994. Averaged equations for inviscid disperse two-phase flow. J. Fluid Mech. 267, 185–220.